

Theoretical and Experimental Evaluation of a Real-Time Corrosion Monitoring System for Measuring Pitting in Aircraft Structures

Douglas Brown¹, Duane Darr², Jefferey Morse³, and Bernard Laskowski⁴

^{1,2,3,4} *Analatom, Inc., 562 E. Weddell Dr. Suite 4, Sunnyvale, CA 94089-2108, USA*

Doug.Brown@analatom.com

Duane.Darr@analatom.com

Jeff.Morse@analatom.com

Bernard.Laskowski@analatom.com

ABSTRACT

This paper presents the theory and experimental validation of Analatom's Structural Health Management (SHM) system for monitoring corrosion. Corrosion measurements are acquired using a micro-sized Linear Polarization Resistance (μ LPR) sensor. The μ LPR sensor is based on conventional macro-sized Linear Polarization Resistance (LPR) sensors with the additional benefit of a reduced form factor making it a viable and economical candidate for remote corrosion monitoring of high value structures, such as buildings, bridges, or aircraft.

A series of experiments were conducted to evaluate the μ LPR sensor for AA 7075-T6. Test coupons were placed alongside Analatom's μ LPR sensors in a series of accelerated tests. LPR measurements were sampled at a rate of once per minute and converted to a corrosion rate using the algorithms presented in this paper. At the end of the experiment, pit-depth due to corrosion was computed for each sensor from the recorded LPR measurements and compared to the average pit-depth measured on the control coupons. The results demonstrate the effectiveness of the sensor as an efficient and practical approach to measuring pit-depth for AA 7075-T6.

1. INTRODUCTION

Recent studies have exposed the generally poor state of our nation's critical infrastructure systems that has resulted from wear and tear under excessive operational loads and environmental conditions. SHM (Structural Health Monitoring) Systems aim at reducing the cost of maintaining high value structures by moving from SBM (Scheduled Based Maintenance) to CBM (Condition Based Maintenance) schemes (Huston, 2010). These systems must be low-cost, simple to install with a user interface designed to be easy to operate. To re-

Douglas Brown et.al. This is an open-access article distributed under the terms of the Creative Commons Attribution 3.0 United States License, which permits unrestricted use, distribution, and reproduction in any medium, provided the original author and source are credited.

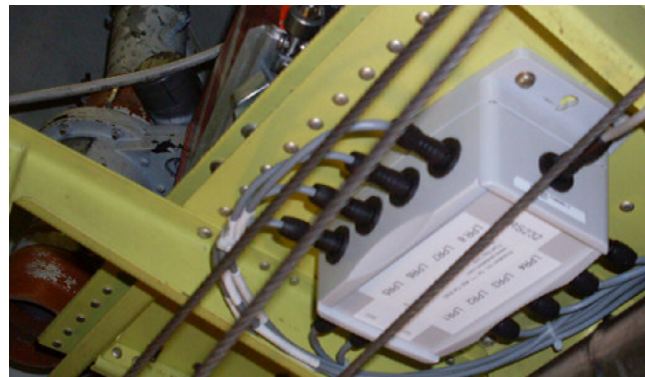


Figure 1. Analatom AN101 SHM system installed in the rear fuel-bay bulkhead of a commercial aircraft.

duce the cost and complexity of such a system a generic interface node that uses low-powered wireless communications has been developed by Analatom. This node can communicate with a myriad of common sensors used in SHM. In this manner a structure such as a bridge, aircraft or ship can be fitted with sensors in any desired or designated location and format without the need for communications and power lines that are inherently expensive and complex to route. Data from these nodes is transmitted to a central communications Personal Computer (PC) for data analysis. An example of this is provided in Figure 1 showing Analatom's AN101 SHM system installed in the rear fuel-bay bulkhead of a commercial aircraft.

A variety of methods such as electrical resistance, gravimetric-based mass loss, quartz crystal micro-balance-based mass loss, electrochemical, and solution analysis methods enable the determination of corrosion rates of metals. The focus of this paper is on, Linear Polarization Resistance (LPR), a method based on electrochemical concepts to determine instantaneous interfacial reaction rates such as corrosion rates and exchange current densities from a single experiment. There are a variety of methods capable of experimen-

tally determining instantaneous polarization resistances such as potential step or sweep, current step or sweep, impedance spectroscopy, as well as statistical and spectral noise methods (Scully, 2000). The remainder of this paper will focus on the former as the AN101 SHM system uses the potential step (or sweep) approach to measure LPR.

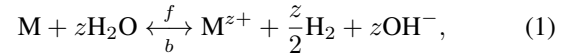
The remainder of the paper is organized by the following. Section 2 describes the general theory governing LPR. Section 3 presents Analatom's μ LPR discussing the benefits of miniaturizing the sensor from a macro-scaled LPR. Section 4 outlines the experimental setup and procedure used to validate the μ LPR sensor. Section 5 presents the experimental measurements with the accompanying analysis which demonstrates the effectiveness of the μ LPR sensor. Finally, the paper is concluded in Section 6 with a summary of the findings and future work.

2. LPR THEORY

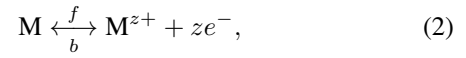
The corrosion of metals takes place when the metal dissolves due to oxidation and reduction (electrochemical) reactions at the interface of metal and the (aqueous) electrolyte solution. Atmospheric water vapor is an example of an electrolyte that corrodes exposed metal surface and wet concrete is another example of an electrolyte that can cause corrosion of reinforced rods in bridges. Corrosion usually proceeds through a combination of electrochemical reactions; (1) anodic (oxidation) reactions involving dissolution of metals in the electrolyte and release of electrons, and (2) cathodic (reduction) reactions involving gain of electrons by the electrolyte species like atmospheric oxygen O_2 , moisture H_2O , or H^+ ions in an acid (Bockris, Reddy, & Gambola-Aldeco, 2000). The flow of electrons from the anodic reaction sites to the cathodic reaction sites constitutes corrosion current and is used to estimate the corrosion rate. When the two reactions are in equilibrium at the equilibrium corrosion potential, E_{corr} , the net current on the metal surface is zero without an external source of current. The anodic reactions proceed more rapidly at more positive potentials and the cathodic reactions proceed more rapidly at more negative potentials. Since the corrosion current from the unstable anodic and cathodic sites is too small to measure, an external activation potential is applied across the metal surface and the current is measured for electrochemical calculations. The resulting E_a vs. I_a curve is called the polarization curve. Under external activation potential, the anodic and cathodic currents increase exponentially and so when $\log_{10} I_a$ is plotted against E_a (a Tafel Plot), the linear regions on the anodic and cathodic curves correspond to regions where either the anodic or cathodic reactions dominate and represent the rate of the electrochemical process. The extrapolation of the Tafel linear regions to the corrosion potential gives the corrosion current, I_{corr} , which is then used to calculate the rate of corrosion (Burstein, 2005).

2.1. Anodic and Cathodic Reactions

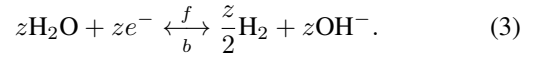
Electrochemical technique of Linear Polarization Resistance (LPR) is used to study corrosion processes since the corrosion reactions are electrochemical reactions occurring on the metal surface. Modern corrosion studies are based on the concept of mixed potential theory postulated by Wagner and Traud, which states that the net corrosion reaction is the result of two or more partial electrochemical reactions that proceed independently of each other (Wagner & Traud, 1938). For the case of metallic corrosion in presence of an aqueous medium, the corrosion process can be written as,



where z is the number of electrons lost per atom of the metal. This reaction is the result of an anodic (oxidation) reaction,



and a cathodic (reduction) reaction,



It is assumed that the anodic and cathodic reactions occur at a number of sites on a metal surface and that these sites change in a dynamic statistical distribution with respect to location and time. Thus, during corrosion of a metal surface, metal ions are formed at anodic sites with the loss of electrons and these electrons are then consumed by water molecules to form hydrogen molecules. The interaction between the anodic and cathodic sites as described on the basis of mixed potential theory is represented by well-known relationships using current (reaction rate) and potential (driving force). For the above pair of electrochemical reactions (anodic (2) and cathodic (3)), the relationship between the applied current I_a and potential E_a follows the Butler-Volmer equation,

$$I_a = I_{corr} \left\{ \exp \left[\frac{2.303 (E_a - E_{corr})}{\beta_a} \right] - \dots \exp \left[-\frac{2.303 (E_a - E_{corr})}{\beta_c} \right] \right\}, \quad (4)$$

where β_a and β_c are the anodic and cathodic Tafel parameters given by the slopes of the polarization curves $\partial E_a / \partial \log_{10} I_a$ in the anodic and cathodic Tafel regimes, respectively and E_{corr} is the corrosion potential (Bockris et al., 2000).

2.2. Electrode Configuration

An electrode is a (semi-)conductive solid that interfaces with an electrolytic solution. The most common electrode configuration is the three-electrode configuration. The common designations are: working, reference and counter electrodes. The working electrode is the designation for the electrode being studied. In corrosion experiments, this is the material that

is corroding. The counter electrode is the electrode that completes the current path. All electrochemistry experiments contain a working-counter pair. In most experiments the counter electrode is simply the current source/sink comprised of inert materials like graphite or platinum. Finally, the reference electrode serves as an experimental reference point, specifically for potential (sense) measurements. The reference electrode is positioned so that it measures a point very close to the working electrode.

The three-electrode setup has a distinct experimental advantage over a two electrode setup: only one half of the cell is measured. That is, potential changes of the working electrode are measured independently of changes that may occur at the counter electrode. This configuration also reduces the effect of measuring potential drops across the solution resistance when measuring between the working and counter electrodes.

2.3. Polarization Resistance

The corrosion current, I_{corr} , cannot be measured directly. However, a-priori knowledge of β_a and β_c along with a small signal analysis technique, known as polarization resistance, can be used to indirectly compute I_{corr} . The polarization resistance technique, also referred to as ‘‘linear polarization’’, is an experimental electrochemical technique that estimates the small signal changes in I_a when E_a is perturbed by $E_{corr} \pm 10$ mV (G102, 1994). The slope of the resulting curve over this range is the polarization resistance,

$$R_p \triangleq \left. \frac{\partial E_a}{\partial I_a} \right|_{|E_a - E_{corr}| \leq 10 \text{ mV}}. \quad (5)$$

Note, the applied current, I_a , is the total applied current and is not multiplied by the electrode area so R_p as defined in (5) has units of Ω . Provided that $|E_a - E_{corr}|/\beta_a \leq 0.1$ and $|E_a - E_{corr}|/\beta_c \leq 0.1$, the first order Taylor series expansion $\exp(x) \approx 1 + x$ can be applied to (4) and (5) to arrive at,

$$R_p = \frac{1}{2.303 I_{corr}} \left(\frac{\beta_a \beta_c}{\beta_a + \beta_c} \right). \quad (6)$$

Finally, this expression can be re-written for I_{corr} to arrive at the Stern-Geary equation,

$$I_{corr} = \frac{B}{R_p}, \quad (7)$$

where $B = \frac{1}{2.303} [\beta_a \beta_c / (\beta_a + \beta_c)]$ is a constant of proportionality.

2.4. Pit Depth

The pit depth due to corrosion is calculated by computing the pitting current density, i_{pit} ,

$$i_{pit}(t) = \frac{i_{corr} - i_{pv}}{N_{pit}}, \quad (8)$$

where $i_{corr} = I_{corr}/A_{sen}$ is the corrosion current density, i_{pv} is the passive current density, N_{pit} is the pit density for the alloy (derived empirically) and A_{sen} is the effective surface area of the LPR sensor. One critical assumption is the pH is in the range of 6-8. If this cannot be assumed, then a measurement of pH is required and $i_{passive}$ is needed over the range of pH values. Next, Faraday’s law is used to relate the total pitting charge with respect to molar mass loss. Let the equivalent weight (EW) represent the weight of the metal that reacts with 1 C of charge, thus contributing to the corrosion and overall loss of material in the anodic (oxidation) reaction given in (2). The total pitting charge, Q_{corr} , and molar mass loss, M , can be related to the following,

$$Q_{pit}(t) = zF \cdot M(t), \quad (9)$$

where $F = 9.650 \times 10^4$ C/mol is Faraday’s constant, and z is the number of electrons lost per atom in the metal in the reduction-oxidation reaction. The EW is calculated from the known Atomic Weight (AW) of the metal,

$$EW = \frac{AW}{z}. \quad (10)$$

Next, the number of moles of the metal reacting can be converted to an equivalent mass loss, m_{loss} ,

$$m_{loss}(t) = M(t) \cdot AW. \quad (11)$$

Combining (9) through (11), the mass loss m_{loss} is related to Q_{pit} by,

$$m_{loss}(t) = \frac{EW \cdot Q_{pit}(t)}{F}. \quad (12)$$

With the mass loss calculated and knowing the density ρ , the pit-depth modeled using a semi-spherical volume with a depth (or radius) d is expressed as,

$$d(t) = \left(\frac{3m_{loss}(t)}{2\pi\rho} \right)^{1/3}. \quad (13)$$

Now, note that Q_{pit} can be found by integrating i_{pit} over the total time,

$$Q_{pit}(t) = \int_0^t i_{pit}(\tau) d\tau, \quad (14)$$

Substituting (12) and (14) into (13) gives,

$$d(t) = \sqrt[3]{\frac{3EW}{2\pi\rho F} \int_0^t i_{pit}(\tau) d\tau}. \quad (15)$$

Next, by substituting (7) and (8) into (15), the expression for d can be rewritten as,

$$d(t) = \sqrt[3]{\frac{3EW}{2\pi\rho N_{pit} F} \int_0^t \left(\frac{B}{A_{sen} R_p(\tau)} - i_{pv} \right) d\tau}. \quad (16)$$

In practice, R_p is not measured continuously, rather, periodic measurements are taken every T_s seconds. If its assumed over this interval the R_p values changes linearly then the mean value theorem for integrals can be applied to arrive at an alternative expression for d ,

$$d(t) = \sqrt[3]{\frac{3T_s EW}{2\pi\rho N_{pit} F} \sum_{k=0}^{N-1} \left(\frac{B}{A_{sen} R_p(kT_s)} - i_{pv} \right)}. \quad (17)$$

2.5. Standard Measurements

Capacitive current can result in hysteresis in small amplitude cyclic voltammogram E_a vs. I_a plots. High capacitance, multiplied by a rapid voltage scan rate, causes a high capacitive current that results in hysteresis in cyclic E_a vs. I_a data (Scully, 2000). This affect can be reduced by making measurements at a slow scan rate. The maximum scan rate allowed to obtain accurate measurements has been addressed by Mansfield and Kendig (Mansfield & Kendig, 1981). The maximum applied frequency allowed to obtain the solution resistance, R_s , and the polarization resistance, R_p , from a Bode plot can be approximated by,

$$f_{\max} < f_{bp} \approx \frac{1}{2\pi C (R_p + R_s)}, \quad (18)$$

where f_{bp} is an approximation of the lower break-point frequency, f_{\max} is the maximum test frequency and C is the capacitance that arises whenever an electrochemical interface exists between the electronic and ionic phases.

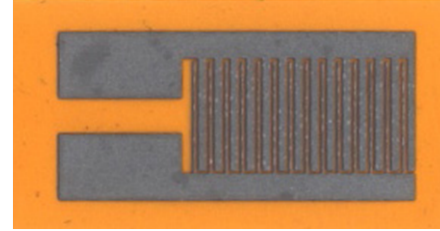
2.5.1. Linear Polarization Resistance (LPR)

ASTM standards D2776 and G59 describe standard procedures for conducting polarization resistance measurements. Potentiodynamic, potential step, and current-step methods can be used to compute R_p (D2776, 1994; G59, 1994). The potentiodynamic sweep method is the most common method for acquiring R_p . For conventional macro-LPR measurements, a potentiodynamic sweep is conducted by applying E_a between $E_{corr} \pm 10$ mV at a slow scan rate, typically 0.125 mV/s. A linear fit of the resulting E_a vs. I_a curve is used to compute R_p . Performing this operation takes 160 seconds to complete.

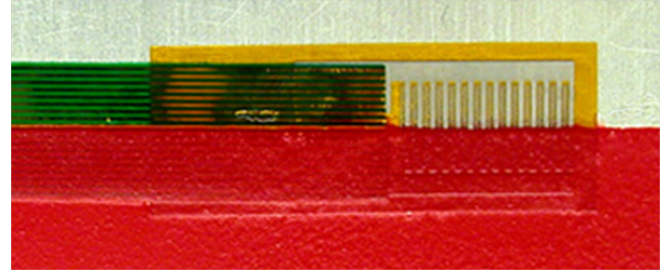
3. μ LPR CORROSION SENSOR

In this section, a micro-LPR (μ LPR) is presented which uses the potential step-sweep method to compute polarization resistance. The μ LPR works on the same principle as the macro-sized LPR sensors and is designed to corrode at the same rate as the structure on which it is placed. Although LPR theory is well established and accepted as a viable corrosion monitoring technique, conventional macro-sized LPR sensor systems are expensive and highly intrusive. The μ LPR is a micro-scaled LPR sensor inspired from the macro-sized version discussed in the previous section. Scaling the LPR sensor into a micro-sized package provides several advantages which include,

- Miniature form factor
- Two-pair electrode configuration
- Faster LPR measurements



(a)



(b)

Figure 2. Thin film μ LPR sensor (a) exposed and (b) quasi-exposed with the lower-half underneath a coating.

3.1. Form Factor

Expertise in semiconductor manufacturing is used to micro-machine the μ LPR. Using photolithography it is possible to manufacture the μ LPR sensor from a variety of standard engineering construction materials varying from steels for buildings and bridges through to novel alloys for airframes. The micro sensor is made up of two micro machined electrodes that are interdigitated at 150 μ m spacing. The μ LPR sensor is made from shim stock of the source/sample material that is pressure and thermally bonded to Kapton tape. The shim is prepared using photolithographic techniques and Electro Chemical Etching (ECM). It is further machined on the Kapton to produce a highly ductile and mechanically robust micro sensor that is very sensitive to corrosion. Images of the μ LPR shown bare and a fitted sensor underneath a coating are shown in Figure 2.

3.2. Electrode Configuration

The μ LPR differs from the conventional macro-sized LPR sensors in two major ways. First, the μ LPR only consists of two electrodes. The need for the reference electrode is eliminated as the separation distance between the working and counter electrodes, typically 150 μ m, minimizes any voltage drop due to the solution resistance, R_s . Second, both electrodes are composed of the same working metal. This is uncommon in most electrochemical cells where the counter electrode is made of an inert material. The benefit is the electrodes provide a more direct measurement of corrosion than techniques which use electrodes made of different metals (eg. gold). The sensor consists of multiple plates made from the material of interest which form the two electrodes. The elec-

trodes are used in conjunction with a potentiostat for conducting LPR measurements. The use of a relatively large counter electrode minimizes polarization effects at the counter electrode to ensure that a stable reference potential is maintained throughout the experiments.

3.3. LPR Measurements

Potential step-sweeps are performed by applying a series of 30 steps over a range of ± 10 mV spanning a period of 2.6 s. This allows eight μ LPR sensors to be measured in less than 30 s. However, the effective scan-rate of 7.7 mV/s generates an additional current, I_{dl} , due to rapid charging and discharging of the capacitance, referred to as the double-layer capacitance C_{dl} , at the electrode-electrolyte interface,

$$I_{dl} = C_{dl} \frac{dE_a}{dt}. \quad (19)$$

Let the resulting polarization resistance that is computed when I_{dl} is non-zero be represented by \hat{R}_p . It can be shown that \hat{R}_p is related to R_p by the following,

$$\hat{R}_p^{-1} = R_p^{-1} + Y_{dl}, \quad (20)$$

such that Y_{dl} is defined by the admittance,

$$Y_{dl} = \left(\frac{C_{dl}}{20 \text{ mV}} \right) \frac{dE_a}{dt} \quad (21)$$

where dE_a/dt is the scan rate. An example of this relationship is provided in Figure 3. In this example $C_{dl}/20$ mV and R_p^{-1} correspond to the slope and y-intercept; these values were computed as $5.466 \times 10^{-8} \text{ } \Omega^{-1} \cdot \text{s/mV}$ and $3.624 \times 10^{-6} \text{ } \Omega$, respectively. For a scan rate of $dE_a/dt = 7.7 \text{ mV/s}$, Y_{dl} is computed as $4.209 \times 10^{-7} \text{ } \Omega^{-1}$. Finally, for a given solution, \hat{R}_p can be compensated by,

$$R_p = \frac{\hat{R}_p}{1 - Y_{dl}\hat{R}_p} \quad \text{for} \quad Y_{dl}R_p < 1. \quad (22)$$

A plot of the actual LPR, R_p , vs. the measured LPR, \hat{R}_p , for a μ LPR sensor made from AA 7075-T6 with at a scan-rate of 7.7 mV/s is provided in Figure 4(a). Note, as \hat{R}_p decreases, the error between R_p and \hat{R}_p also decreases, shown in Figure 14(b). This is significant for the following reasons:

- Better accuracy is necessary for smaller values of \hat{R}_p as the corrosion rate increases with R_p^{-1}
- When \hat{R}_p is large, the corrosion rate approaches zero. Therefore, even as the error in R_p increases substantially, the error in the corrosion rate becomes negligible.
- The corrosion rate computed using \hat{R}_p will over-estimate the actual corrosion rate computed from R_p .

Due to these reasons, and the fact that Analatom's AN101 has an upper limit of $5 \text{ M}\Omega$ for measuring \hat{R}_p , no compensation is performed when computing corrosion rates.

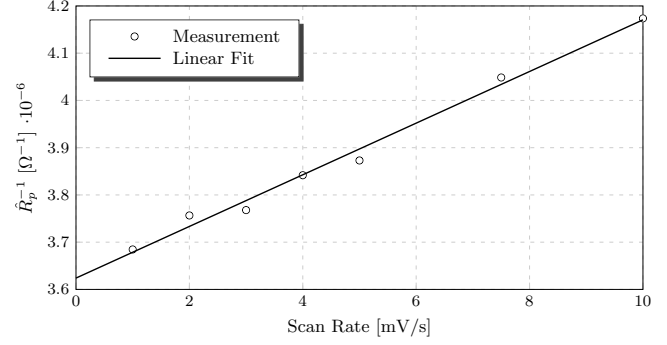


Figure 3. Plot of inverse polarization resistance vs. scan-rate for a μ LPR sensor made from AA 7075-T6 submerged in tap water.

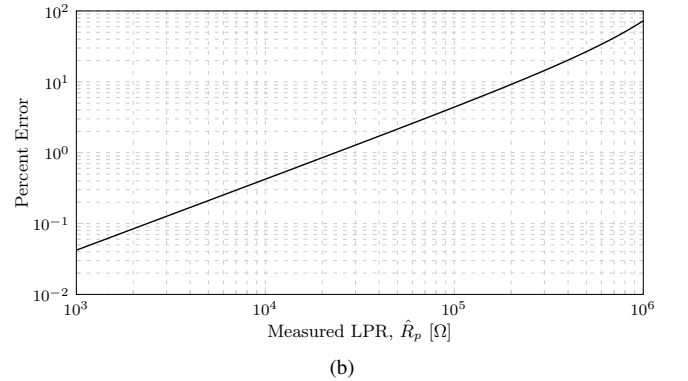
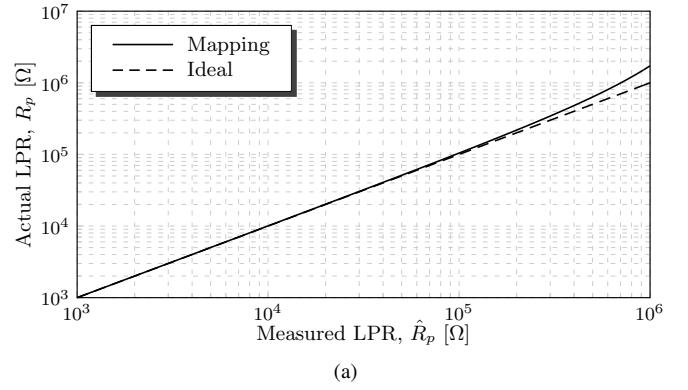


Figure 4. Plot of the (a) actual LPR, R_p , vs. the measured LPR, \hat{R}_p , and (b) corresponding measurement error for a μ LPR sensor made from AA 7075-T6 with at a scan-rate of 7.7 mV/s.

3.4. Maximum Scan Rate

The maximum measurement speed for conventional macro-sized LPR systems is restricted by the combination of resistance (solution / polarization) and capacitance at the electrochemical interface. From (18), f_{max} can be determined graphically by estimating f_{bp} from a Bode plot. A bode plot for the magnitude and phase response of a μ LPR sensor constructed from AA 7075-T6 submerged in distilled water is

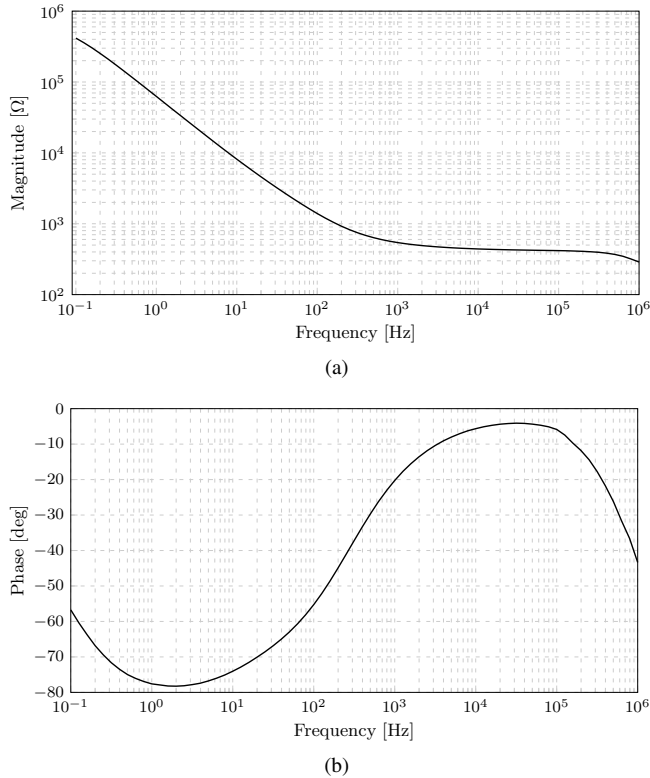


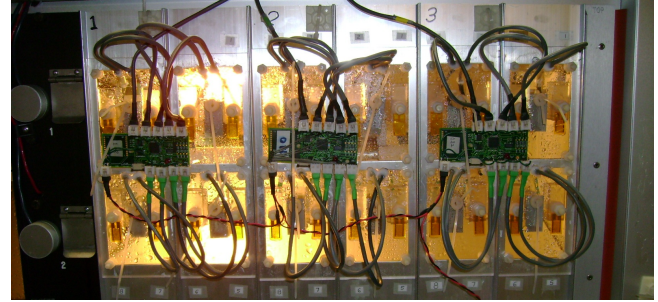
Figure 5. Bode plot showing the (a) magnitude and (b) phase for a μ LPR sensor constructed from AA 7075-T6 with distilled water as the electrolyte.

shown in Figure 5. The data was generated using a potentiostat over the frequency range 0.1 Hz – 1 MHz. The magnitude response can be used to measure $f_{bp} > 100$ Hz. In practice, the μ LPR sensor applies a scan rate of 7.7 mV/s with a step-size of 0.67 mV between samples. This is equivalent to a sampling rate of 11.5 Hz which is a factor of ten less than f_{bp} .

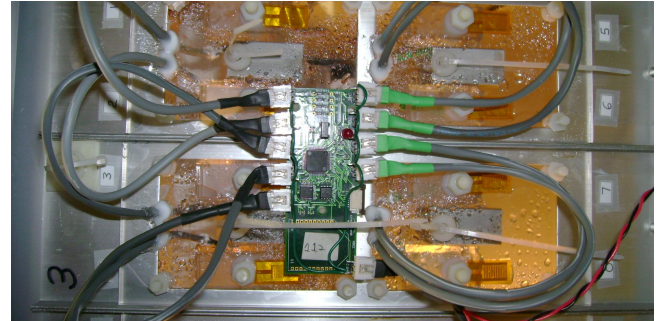
4. EXPERIMENT

4.1. Setup

The experiment consisted of twenty-four (24) μ LPR sensors and twelve (12) control coupons. The coupons and μ LPR sensors were made from AA 7075-T6. Each coupon was placed next to a pair of μ LPR sensors. Each sensor was held in place using a non-reactive polycarbonate clamp with a nylon fitting. All the sensors and coupons were mounted on an acrylic plexiglass base with the embedded hardware placed on the opposite side of the frame, shown in Figure 6. An electronic precision balance (Tree HRB-203) with a calibrated range of 0 – 200 g (± 0.001 g) was used to weigh the coupons before and after the experiment. Finally, a weathering chamber (Q-Lab QUV/spray) promoted corrosion on the coupons and μ LPR sensors by applying a controlled stream of tap water for 10 seconds every five minutes.



(a)



(b)

Figure 6. Experimental setup showing (a) all 24 μ LPR sensors, 12 coupons and three AN101 instrumentation boards and (b) a close-up view of one of the panels used in the experiment. *Note: only the first six coupons were used in the analysis performed in this paper.*

4.2. Procedure

First, the surface of each coupon was cleaned using sand-blasting. Then, each coupon was weighed using the analytical balance. The entire panel of coupons and μ LPR sensors were placed in the weathering chamber for accelerated testing. The experiment ran for approximately 35 days. During the experiment, a set of coupons were periodically removed from the weathering chamber. Throughout the experiment, Analom's embedded hardware was logging \hat{R}_p from each μ LPR sensor. The sample rate was set at one sample per minute. Once accelerated testing was finished, the coupons were removed and the LPR data was downloaded and archived for analysis. The corrosion byproducts were removed from each coupon by applying micro-bead blasting to the coupon surface. Finally, the cleaned coupons were weighed using the analytical scale to compute the relative corrosion depth during the experiment.

5. RESULTS

5.1. Coupon Corrosion

The corrosion byproducts were carefully removed using micro-bead blasting. The pitting depth, d , of each coupon

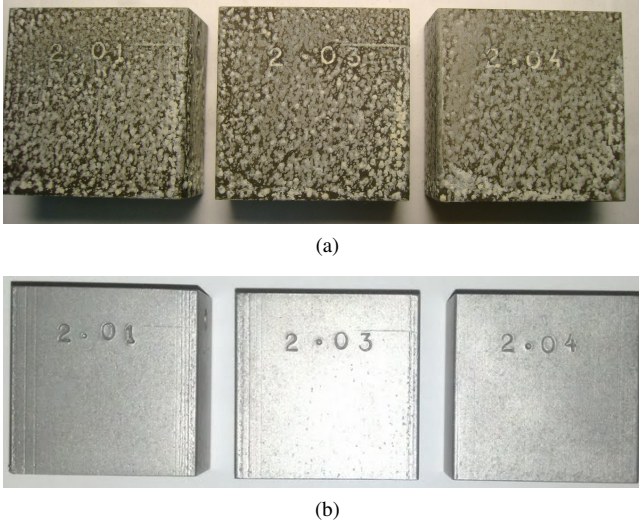


Figure 7. Image of the three AA 7075-T6 coupons (ID 2.01, 2.03 and 2.04) after approximately 17 days of corrosion testing showing (a) the condition of the coupons before cleaning and (b) after cleaning using micro-bead blasting.

was calculated using the formula,

$$d = \sqrt[3]{\frac{3m_{loss}}{2\pi\rho N_{pit}A_{exp}}}, \quad (23)$$

where values for the mass loss m_{loss} , exposed surface area A_{exp} , resulting pit depth, d , and total time of exposure of each coupon is provided in Table 1. Values for the pitting density and ρ were set at $N_{pit} = 10 \text{ cm}^{-2}$ and $\rho = 2.810 \text{ g/cm}^3$, respectively. The pitting density was computed by counting the average number of pits over the surface for coupons 2.06 and 2.08. The measurement uncertainty in the pit-depth due to uncertainty in the mass loss, Δm_{loss} and pit density, ΔN_{pit} , is approximately,

$$\Delta d \approx \frac{d}{3} \left(\frac{\Delta m_{loss}}{m_{loss}} + \frac{\Delta N_{pit}}{N_{pit}} \right), \quad (24)$$

where $\Delta m_{loss} = \pm 0.001 \text{ g}$ is the minimum resolution of the scale and $\Delta N_{pit} = \pm 3 \text{ cm}^{-2}$ was the standard deviation of the measured pit density over 1 cm^2 sample areas for coupons 2.06 and 2.08.

5.2. μ LPR Corrosion

The linear polarization resistance measurements were used to compute corrosion pit depth for each μ LPR sensor. The computed pit-depth for each of the 24 μ LPR sensors is provided in Figure 8.

6. SUMMARY

A micro-sized LPR (μ LPR) sensor was presented for corrosion monitoring in Structural Health Management (SHM) applications. An experimental test was performed to com-

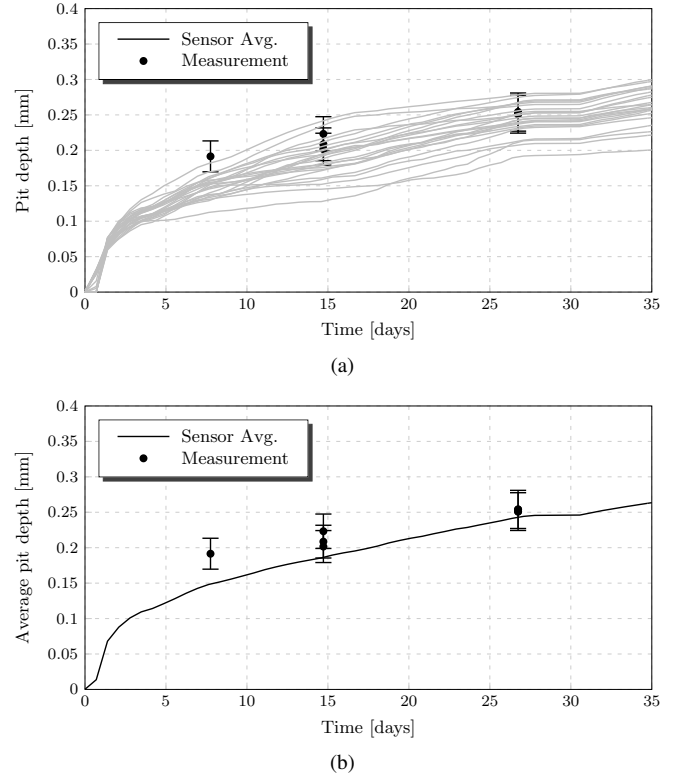


Figure 8. Comparison of the measured and computed pit depth over a period of approximately 35 days for (a) each μ LPR sensor and (b) the average of all μ LPR sensors.

pare corrosion measurements from twenty-four μ LPR sensors with twelve coupons. Both the coupons and sensors were constructed from the same material, AA 7075-T6. According to the results, the pit-depth measured on the coupons fell within the 95% confidence interval computed from the pit-depth measured on the μ LPR sensors. The results indicate multiple μ LPR can be used to provide an accurate measurement of corrosion. Future work includes testing additional alloys such as AA 7075-T6 and performing in-flight testing on a C-130 legacy aircraft.

ACKNOWLEDGMENT

All funding and development of the sensors and systems in the project has been part of the US government's SBIR programs. In particular: 1) In preparing the initial system design and development, funding was provided by the US Air Force under SBIR Phase II contract # F33615-01-C-5612 monitored by Dr. James Mazza, 2) Funding for the development and experimental set-up was provided by the US Navy under SBIR Phase II contract # N68335-06-C-0317 monitored by Dr. Paul Kulowitch, and 3) for further improvements and scheduled field installations by the US Air Force under SBIR Phase II contract # FA8501-11-C-0012 monitored by Mr. Feraiidooon Zahiri.

Table 1. Experimental measurements of coupon corrosion.

Coupon ID	Time Exposed [min]	Area [cm ²]	Initial Mass [g]	Final Mass [g]	Mass Loss [g]	Pit Depth [mm]
Control	0	5.801×10^1	7.6870×10^1	7.6869×10^1	1×10^{-3}	N/A
2.01	2.1198×10^4	5.805×10^1	7.7253×10^1	7.7215×10^1	3.8×10^{-2}	2.162×10^{-1}
2.02	1.1160×10^4	5.798×10^1	7.6842×10^1	7.6818×10^1	2.4×10^{-2}	1.855×10^{-1}
2.03	2.1198×10^4	5.799×10^1	7.6927×10^1	7.6896×10^1	3.1×10^{-2}	2.020×10^{-1}
2.04	2.1198×10^4	5.805×10^1	7.6897×10^1	7.6869×10^1	2.8×10^{-2}	1.953×10^{-1}
2.06	3.8510×10^4	5.798×10^1	7.6884×10^1	7.6828×10^1	5.6×10^{-2}	2.461×10^{-1}
2.08	3.8510×10^4	5.803×10^1	7.6921×10^1	7.6810×10^1	5.4×10^{-2}	2.431×10^{-1}

NOMENCLATURE

β_a	Anodic Tafel slope	V/dec
β_c	Cathodic Tafel slope	V/dec
ρ	Density	g/mm ³
d	Corrosion depth	cm
k	LPR sample index	–
f_{bp}	Break-point frequency	Hz
f_{max}	Maximum test frequency	Hz
i_{corr}	Corrosion current density	A/cm ²
i_{pit}	Pitting current density	A/cm ²
i_{pv}	Passive current density	A/cm ²
m_{loss}	Mass loss due to corrosion	g
z	Number of electrons lost per atom	–
Δd	Corrosion depth uncertainty	cm
Δm_{loss}	Mass loss uncertainty	g
ΔN_{pit}	Pit density uncertainty	cm ⁻²
A_{sen}	Effective sensor area	cm ²
A_{exp}	Exposed coupon area	cm ²
AW	Atomic Weight	g/mol
B	Proportionality constant	V/dec
C_{dl}	Double-layer capacitance	F
E_a	Applied potential	V
E_{corr}	Corrosion voltage	V
EW	Equivalent weight	g/mol
F	Faraday's constant	C/mol
I_a	Applied current	A
I_{dl}	Scanning current from C_{dl}	A
I_{corr}	Corrosion current	A
M	Number of moles reacting	mol
N	Total number of μ LPR samples	–
N_{pit}	Pit density	cm ⁻²
Q_{corr}	Charge from oxidation reaction	C
R_p	Polarization resistance	Ω
\hat{R}_p	Measured polarization resistance	Ω
R_s	Solution resistance	Ω
T_s	Sampling period	s
Y_{dl}	Scanning admittance from C_{dl}	s

REFERENCES

- Bockris, J. O., Reddy, A. K. N., & Gambola-Aldeco, M. (2000). *Modern Electrochemistry 2A. Fundamentals of Electrodeics* (2nd ed.). New York: Kluwer Academic/Plenum Publishers.
- Burstein, G. T. (2005, December). A Century of Tafel's Equation: 1905-2005. *Corrosion Science*, 47(12), 2858-2870.
- D2776, A. S. (1994). Test Methods for Corrosivity of Water in the Absence of Heat Transfer. *Annual Book of ASTM Standards*, 03.02.
- G102, A. S. (1994). Standard Practice for Calculation of Corrosion Rates and Related Information from Electrochemical Measurements. *Annual Book of ASTM Standards*, 03.02.
- G59, A. S. (1994). Standard Practice for Conducting Potentiodynamic Polarization Resistance Measurements. *Annual Book of ASTM Standards*, 03.02.
- Huston, D. (2010). *Structural Sensing, Health Monitoring, and Performance Evaluation* (B. Jones & W. B. S. J. Jnr., Eds.). Taylor and Francis.
- Mansfeld, F., & Kendig, M. (1981). *Corrosion*, 37, 545.
- Scully, J. R. (2000, February). Polarization Resistance Method for Determination of Instantaneous Corrosion Rates. *Corrosion*, 56(2), 199-218.
- Wagner, C., & Traud, W. (1938). *Elektrochem*, 44, 391.

Douglas W. Brown is the senior systems engineer at Analatom with eight years of experience developing and maturing PHM and fault-tolerant control systems in avionics applications. He received the B.S. degree in electrical engineering from the Rochester Institute of Technology in 2006 and the M.S/Ph.D. degrees in electrical engineering from the Georgia Institute of Technology in 2008 and 2011, respectively. Dr. Brown is a recipient of the National Defense Science and Engineering Graduate Fellowship and has re-

ceived several best-paper awards in his work in prognostics and fault-tolerant control.

Duane Darr is the senior embedded hardware engineer at Analatom with over 30 years of experience in the software and firmware engineering fields. He completed his undergraduate work in physics, and graduate work in electrical engineering and computer science at Santa Clara University. Mr. Darr's previous work at Epson Imaging Technology Center, San Jose, California, as Senior Software Engineer, Data Technology Corporation, San Jose, California as Senior Firmware Engineer, and Qume Inc., San Jose California, as Member of Engineering Staff/Senior Firmware Engineer, focused on generation and refinement of software and firmware solutions for imaging core technologies as well as digital servo controller research, development, and commercialization.

Jefferey Morse is the director of advanced technology at Analatom since 2007. Prior to this, he was a senior scientist in the Center for Micro and Nano Technology at Lawrence Livermore National Laboratory. He received the B.S. and

M.S. degrees in electrical engineering from the University of Massachusetts Amherst in 1983 and 1985, respectively, and a Ph.D. in electrical engineering from Stanford University in 1992. Dr. Morse has over 40 publications, including 12 journal papers, and 15 patents in the areas of advanced materials, nanofabrication, sensors and energy conversion technologies. He has managed numerous projects in various multidisciplinary technical areas, including electrochemical sensors and power sources, vacuum devices, and microfluidic systems.

Bernard Laskowski is the president and senior research scientist at Analatom since 1981. He received the Licentiaat and Ph.D. degrees in Physics from the University of Brussels in 1969 and 1974, respectively. Dr. Laskowski has published over 30 papers in international refereed journals in the fields of micro physics and micro chemistry. As president of Analatom, Dr. Laskowski managed 93 university, government, and private industry contracts, receiving a U.S. Small Business Administration Administrator's Award for Excellence.